Continuum Mech. Thermodyn. (2023) 35:1481–1494
https://doi.org/10.1007/s00161-022-01154-z

ORIGINAL ARTICLE

M. Erden Yildizdag · Luca Placidi · Emilio Turco

Modeling and numerical investigation of damage behavior in pantographic layers using a hemivariational formulation adapted for a Hencky-type discrete model

Received: 10 May 2022 / Accepted: 15 September 2022 / Published online: 5 October 2022

Abstract In this study, a hemivariational formulation is presented for a Hencky-type discrete model to predict damage behavior in pantographic layers. In the discrete model, elastic behavior of pantographic layers is modeled via extensional, bending and shear springs. A damage descriptor is added for each spring type. Such a damage descriptor is non-decreasing function of time, and therefore, the standard variational formulation of the problem is generalized to a hemivariational one providing not only the Euler–Lagrange equations for the evolution of the displacements of all the standard degrees of freedom but also the Karush–Khun–Tucker condition governing the evolution of damage descriptor. The dissipation energy included in the hemivariational formulation depends upon six additional constitutive parameters (two per each spring type), and the mechanical behavior of layer is simulated with an efficient and smart strategy able to solve the nonlinear equilibrium equations coupled with the evolution of damage variables. A metallic pantographic layer which was experimentally investigated in the literature is considered to test the proposed formulation.

Keywords Pantographic structures · Discrete model · Hemivariational formulation · Damage · Metamaterials

1 Introduction

In the last decade, new advanced manufacturing processes like 3-D printing have considerably changed the perspective of industrial design applications due to their ability to fabricate complex materials showing unconventional and exotic behaviors [1]. Therefore, design and fabrication of metamaterials has recently become a popular academic and industrial research subject, and a broad range of studies has been presented to assess the versatility of various metamaterials and their potential applications (for example, see [2–6] for different examples).

Communicated by Andreas Öchsner.

M. E. Yildizdag
International Research Center for the Mathematics and Mechanics of Complex Systems, University of L'Aquila, L'Aquila, Italy

M. E. Yildizdag (✉)
Faculty of Naval Architecture and Ocean Engineering, Istanbul Technical University, Istanbul, Turkey
E-mail: yildizdag@itu.edu.tr

L. Placidi
Engineering Faculty, International Telematic University Uninettuno, Rome, Italy
E-mail: luca.placidi@uninettunouniversity.net

E. Turco
Department of Architecture, Design and Urban Planning, University of Sassari, Alghero, Italy
E-mail: eturco@uniss.it

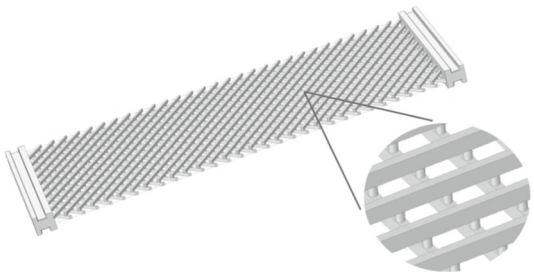

Fig. 1 Topology of pantographic layers

The central theme of this study is to model and investigate damage phenomenon in structural behavior of pantographic metamaterials, which is a type of mechanical metamaterial. In general, a metamaterial is referred to as mechanical metamaterial if its desired overall behavior is obtained as a result of mechanical interaction of structural constituents at different length scales [7]. A standard pantographic layer has two orthogonally aligned fiber families connected by pivots as shown in Fig. 1. Due to its distinctive properties in terms of fabrication, mathematical modeling and mechanical behavior, pantographic layers have been extensively studied in the literature (for instance, see [8–14]). First of all, a pantographic layer can be easily modeled in a CAD software and additively manufactured even with regular 3-D printers. Second, it can be subjected to large deformations while retaining elastic behavior, which may be an interesting property for various engineering applications [15,16]. Third, from a theoretical standpoint, fabrication of pantographic layers has also revealed the applicability of higher-gradient mathematical models. In these models, deformation energy is assumed to be a function of higher gradients of displacement field as opposed to the classical continuum theory (i.e., Cauchy Continuum) [17,18]. This fact has garnered a lot of attention by researchers, and higher-gradient modeling approaches have been utilized to investigate various phenomena such as buckling [19–21], damage and fracture [22–27], and plasticity [28–30]. For interested readers, we refer to the recent works of Abali et al. [31], Barchiesi et al. [32], Spagnuolo et al. [33] and Yang et al. [34] for further details on the applications of higher-gradient mathematical modeling.

In order to investigate the mechanical behavior of a pantographic layer numerically, three different approaches may be followed. If the classical theory is preferred, one should create an appropriate 3-D finite element model of the structure, discretizing all the fibers and pivots with suitable volume elements. Alternatively, one can adapt beam elements, e.g., see [35], to model fibers. However, in this approach, attention must be paid to include the behavior due to the existence of pivots, which is highly crucial in the overall mechanical behavior of pantographic structures as it is highlighted in the literature [36,37]. Besides, second-gradient continuum models can be an alternative to investigate pantographic structures [38–40]. It has been shown that second-gradient models provide a substantial improvement and simplicity in terms of computational cost and discretization to conduct numerical simulations [41]. In addition to numerical approaches based on continuum theory, pantographic structure can also be modeled as a discrete system. In the latter approach, the discrete system is created by assigning a set of particles, and mechanical behaviors of fibers and pivots are modeled by defining suitable linear and rotational springs between particles (see [42–46] for more detail on the discrete modeling approach).

In this study, damage phenomenon occurring in pantographic layers is modeled and examined with a hemivariational formulation. As a target problem, shear test of a metallic pantographic layer consisting of "quasi-perfect" pivots is considered. The current numerical framework accounting damage behavior is an extension of a well-known 2D Hencky-type discrete model developed for pantographic layers. The discrete model includes three mechanical phenomena, namely extension and bending of fibers and torsion of pivots, by suitable linear and rotational springs. To include damage in the problem, a dissipation energy for each type of spring is identified within the hemivariational formulation, which results in additional two constitutive parameters to characterize damage in each kind of spring: one of them corresponds to an activation threshold of damage phenomenon, and the other one prescribes the inertia of damage evolution until fracture. In order to show the applicability of the numerical framework, the specimen under study has been numerically investigated by suitable constitutive parameters, and the obtained numerical force–displacement behavior has been compared to those experimentally measured.

The rest of the paper is as follows. The discrete model and its numerical solution procedure are presented, respectively, in Sects. 2 and 3. Then, the hemivariational formulation to model damage phenomenon is presented

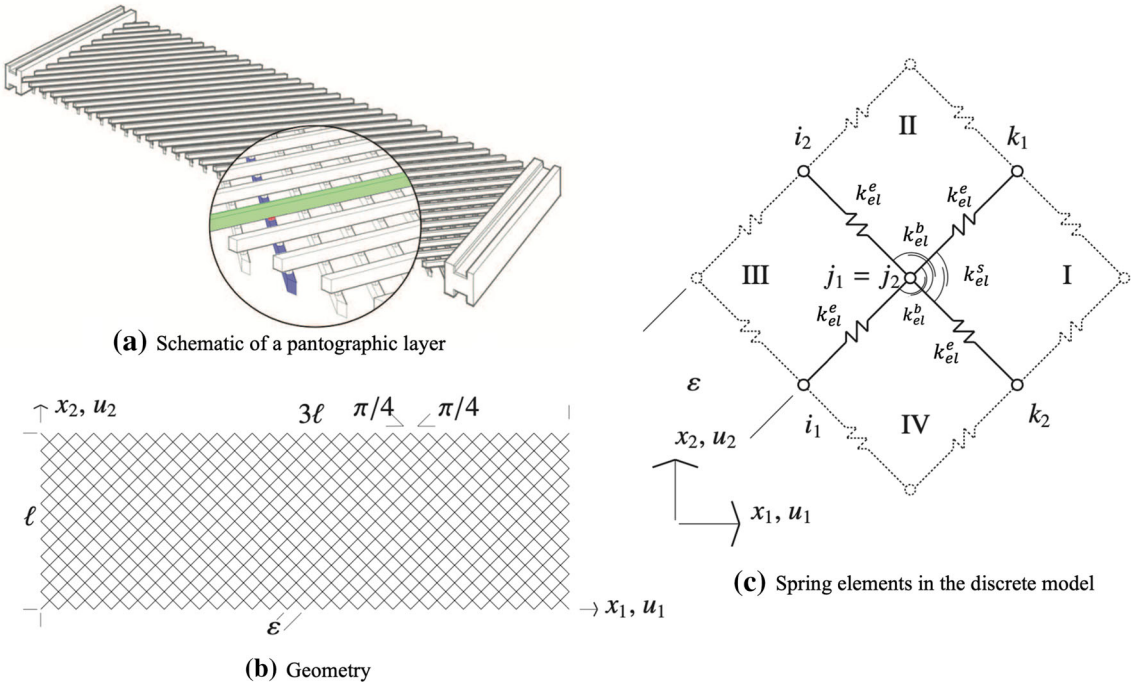

Fig. 2 A pantographic layer and its discrete model: (**a**) Schematic of a pantographic layer with 10 square cells on shorter side and aspect ratio of 3; (**b**) planar lattice geometry being x_1 and x_2 the pivot's position in the reference configuration and u_1 and u_2 displacement components; (**c**) discrete model adopted with suitable spring elements

in Sect. 4, and a numerical study conducted for a metallic pantographic layer is given in Sect. 5. Finally, conclusions are drawn in Sect. 6.

2 Modeling planar pantographic layers following Hencky's pattern

In this section, we synthetically state the model used to describe the mechanical behavior of a pantographic layer such as that depicted in Fig. 2. Here, among many possibilities, we have chosen to model the planar pantographic layer introducing a well-experienced finite dimensional Lagrangian model, see, e.g., [42]. Following Piola, we consider a finite number of material particles occupying, in the reference configuration, the nodes of a rectangular lattice made up of square cells having length ε (see Fig. 2 for a schematic of a pantographic layer of with 10 square cells on the shorter side and aspect ratio of 3).

The pantographic lattice is constituted by two arrays of orthogonal beams, oriented at an angle $\pi/4$ and $-\pi/4$ with respect to x_1 axis. We indicate with 1 the array corresponding to the angle $\pi/4$ (green color) and with 2 the array at the other one (blue color). Each of introduced material particles model the pivots (red color) which, see again Fig. 2a, in the 3D printed specimen link the two arrays of beams.[1]

We introduce the reference position of the generic i-th material particle using their position P_i, whereas the current position of the same material particle is denoted by p_i. This model follows the pioneering work of Hencky [48] and some more recent works [49,50]) for Elasticae. In brief, we model the elastic interactions among the particles by means of extensional and rotational springs, see Fig. 2c, so that pairwise and triple particles interactions appear. The model is completely defined by the strain energy of each one spring. The search of equilibrium configurations is successively solved by imposing the stationarity of potential energy following the algorithm described in Sect. 3.

Our choice for strain energies can be listed below:

[1] The hypothesis of pantographic layer with orthogonal beams can easily be removed as proven in [47].

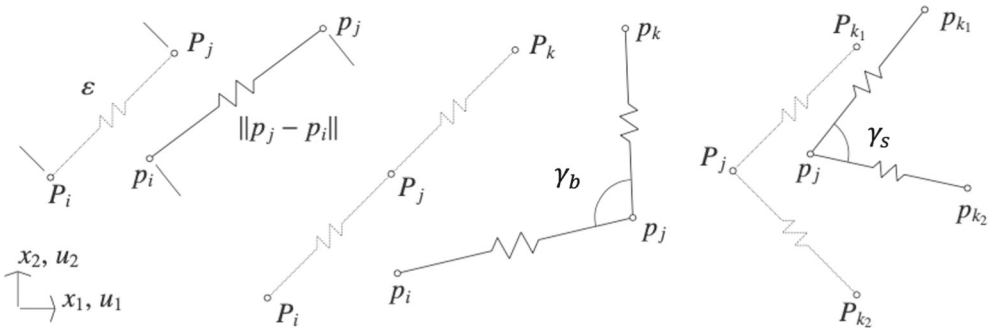

Fig. 3 Kinematics of extensional (on the left), bending (on the middle) and shear (on the right) springs (reference and current configurations are indicated by using upper case and lower case letters)

Strain energy for extensional springs Each extensional spring stores, elastically, an energy which depends quadratically on its length variation:

$$w_{el}^{e} = \frac{1}{2} k_{el}^{e} \left(\| p_j - p_i \| - \varepsilon \right)^2 , \tag{1}$$

where p_i and p_j are the current positions, see Figs. 2c and 3, of the nodes connected by the considered extensional spring whose stiffness is k_{el}^{e}.

Strain energy for bending springs Three consecutive particles along array 1 or 2 interact by means of a rotational spring whose stored elastic energy depends on the angle in between the two consecutive segments connecting, in the current configurations, the particles' positions:

$$w_{b}^{el} = k_{b}^{el} \left(\cos \gamma_b + 1 \right) , \tag{2}$$

where the term $\cos \gamma_b$ is computed by using Carnot's theorem by using the actual positions of aligned nodes (p_{i_1}, p_{j_1}, p_{k_1} for array 1 and p_{i_2}, p_{j_2}, p_{k_2} for array 2) and k_{b}^{el} denote the stiffness of the rotational spring.
Strain energy for shear springs Since the pivots link the two arrays of beams, then the elastic interaction is connected to the current angle γ_s in between the two arrays. Hence we assume that the stored elastic energy depends quadratically on the difference $\left(\gamma_s - \frac{\pi}{2} \right)$

$$w_{s}^{el} = \frac{1}{2} k_{el}^{s} \left(\gamma_s - \frac{\pi}{2} \right)^2 , \tag{3}$$

where (see Figs. 2c and 3) the angle γ_s can be again identified by the Carnot's theorem. In quadrant I, p_{j_1} and p_{k_1}, p_{k_2} are the actual positions of the nodes relative to the rotational spring of stiffness k_{el}^{s} connecting array 1 with array 2. Remark that we assumed to have one exactly equal shear springs also in the quadrants II, III and IV, see Fig. 2c.

The three aforementioned strain energies completely define the Hencky-type model for the planar deformation of pantographic layer accounting extension and bending of fibers and torsion of pivots, and the total strain energy can be obtained simply by summing each contribution. In order to have a complete solution of the considered equilibrium problem, displacements and forces or couples exerted by each spring, a step-by-step procedure was implemented to reconstruct the complete equilibrium path of the pantographic layer, as will be described in detail in the following Sect. 3.

3 Coding a smart strategy able to solve the nonlinear equilibrium equations

The pantographic layer model briefly sketched in Sect. 2 aims to solve problems involving large displacements. For this reason, it is necessary, a specific algorithm able to solve strongly nonlinear problems. We intend, for its generality, to tackle the problem following a step-by-step procedure. In order to code this strategy, we need9 three basic tools: (i) the definition of the structural response vector, in brief the reaction, (ii) the tangent stiffness matrix and (iii) the external load vector.

Starting from the nonlinear system of equilibrium equations obtained by imposing the variation of the total energy

$$\mathbf{s}(\mathbf{u}) - \mathbf{f} = \mathbf{0} \tag{4}$$

where $\mathbf{s}$ is the structural reaction, in brief the reaction, depending from the vector $\mathbf{u}$ which stores the Lagrangian parameters using to describe the motion (nodal displacements) and $\mathbf{f}$ is the vector which collects the external loads.

We firstly calculate the reaction vector $\mathbf{s}$ simply using

$$\mathbf{s} = \nabla E\,, \tag{5}$$

where the ∇ operator embraces the derivatives of the strain energy E respect to the Lagrangian parameters which govern the motion, i.e., the nodal displacements of the pantographic lattice collected in the vector $\mathbf{u}$. Analogously, the work of the external loads W gives

$$\mathbf{f} = \nabla W\,. \tag{6}$$

In order to complete the tools, besides the reaction and the external force vectors, we need definition of the tangent stiffness matrix, or, in other words, the Hessian $H(\cdot)$ of the strain energy E or, equivalently, the gradient of the reaction $\mathbf{s}$

$$\mathbf{K} = H(E) = \nabla \mathbf{s}\,. \tag{7}$$

From a computational point of view, it is convenient to compute with an algebraic manipulator the exact solution corresponding to the elementary cases reported in Fig. 3. Successively, the elementary contributions can be assembled in the global vectors $\mathbf{s}$ and $\mathbf{f}$ and matrix $\mathbf{K}$ by using the same procedure usual in the framework of finite elements. For this work, in order to avoid complex checks on the formulae obtained from the algebraic manipulator, a chip of MATLAB® code producing all the functions necessary to perform the required calculations was built. This in order to save time and to have a optimized and error-free code. In different and rough terms, we built a very small piece of code capable to write the core of the analysis procedure.

The used analysis strategy is essentially founded on the classic Newton's iterative scheme. Since it is well known that the Newton's scheme is not capable to overcome limit points, i.e., points where the stiffness matrix becomes singular, then it is used only as *predictor* leaving the role of *corrector* to the Riks' arc-length strategy [51]. The main aspects of this procedure are well defined in [52] for the limit analysis of Kirchhoff plates and in [43,44] for a pantographic layer modeled as an assembly of springs.

In the framework of a stepwise strategy, the reconstruction of the equilibrium path starts from the knowledge of the curve point—as Newton's scheme require—and computes the following (sufficiently near to the initial).

We assume that the external load be controlled by a scalar parameter λ, i.e., $\mathbf{f}(\lambda) = \lambda\bar{\mathbf{f}}$. It follows that the nonlinear system of equilibrium equations is

$$\mathbf{s}(\mathbf{u}) - \lambda\bar{\mathbf{f}} = \mathbf{0}\,, \tag{8}$$

If the pair $(\lambda_1, \mathbf{u}_1)$ belongs to the equilibrium path, i.e., a measure of the rest of equilibrium equations is near to zero, then a nearby point of the equilibrium path $(\lambda_2, \mathbf{u}_2)$ can be calculated—using the first-order approximation of the rest, i.e., *á la* Newton—by the following iterative scheme:

$$\Delta\mathbf{u} := \mathbf{u}_2 - \mathbf{u}_1 = -\mathbf{K}_{\mathbf{u}_1}^{-1}\left(\mathbf{s}_{\mathbf{u}_1} + (\lambda_1 + \Delta\lambda)\bar{\mathbf{f}}\right)\,, \tag{9}$$

where $\Delta\lambda = \lambda_2 - \lambda_1$ and the vector $\mathbf{s}_{\mathbf{u}_1}$ and the matrix $\mathbf{K}_{\mathbf{u}_1}$ are the reaction and the tangent stiffness matrix computed in $\mathbf{u}_1$, respectively.

In order to overcome the aforementioned limitation of the Newton's scheme, Riks' arc-length strategy, using exactly the same tools, changes essentially the point of view using as parameter to describe the equilibrium path its arc-length, see [51]. In simple words, the equilibrium path is recovered introducing an additional parameter, the curve arc-length, for describing it. The consequent algorithm does not suffer of the Newton's scheme drawback, i.e., no convergence problem arises when the stiffness matrix becomes singular. More details of an smart implementation of the arc-length scheme can be found in [43,45,53]. Here, we describe only some details showing the simplicity and the efficiency of the algorithm.

As mentioned above, the key idea of the Riks' arc-length method is the description of the equilibrium path using, instead of the non-dimensional load parameter λ, its arc-length. As a consequence, the method moves forward on the basis of a fixed arc-length instead of increasing λ. Naturally, since we increase the number of unknown quantities, i.e., the arc-length parameter, a new equation balancing the unknowns is necessary. This simple but fruitful idea permits many different possible choices producing more or less clever algorithms. Probably, the most natural choice is to search the solution on the circle of radius equal to the desired arc-length. At this choice, even if it is surely rigorous, does not follow the faster algorithm. It is much more simple and computationally efficient to code as a rule a kind of orthogonality between the extrapolation, predictor step, and the correction, corrector step. This is equivalent to constrain that the arc-length be constant only in an approximate way.

Starting from the rest of the equilibrium equations:

$$\mathbf{r}(\mathbf{u}_1 + \Delta\mathbf{u} + \dot{\mathbf{u}}, \lambda_1 + \Delta\lambda + \dot{\lambda}) \approx \mathbf{s}_{\mathbf{u}_1+\Delta\mathbf{u}} + \mathbf{K}_{\mathbf{u}_1+\Delta\mathbf{u}}\dot{\mathbf{u}} + (\lambda + \Delta\lambda + \dot{\lambda})\bar{\mathbf{f}} = \mathbf{0}\,, \tag{10}$$

where the pair $(\dot{\lambda}, \dot{\mathbf{u}})$ is the desired correction to the computed extrapolation $(\lambda_1 + \Delta\lambda, \mathbf{u}_1 + \Delta\mathbf{u})$.

The number of equations and that of unknowns have to be balanced; therefore, we must write one additional constraint equation. A quite general form is

$$\Delta\mathbf{u}^T\mathbf{C}\dot{\mathbf{u}} + \gamma\Delta\lambda\dot{\lambda} = 0\,, \tag{11}$$

where, besides the already defined quantities, the matrix $\mathbf{C}$ and the scalar γ appear. The matrix $\mathbf{C}$ and scalar γ can be chosen, e.g., to improve the convergence or to make simple the calculations. We remark that the condition (11) is rather general and can be interpreted as an orthogonality condition between extrapolation, i.e., the pair $(\Delta\lambda, \Delta\mathbf{u})$, and the correction, i.e., the pair $(\dot{\lambda}, \dot{\mathbf{u}})$.

From Eq. (10), we can compute $\dot{\mathbf{u}}$:

$$\dot{\mathbf{u}} = -\mathbf{K}^{-1}_{\mathbf{u}_1+\Delta\mathbf{u}}\left(\mathbf{s}_{\mathbf{u}_1+\Delta\mathbf{u}} + (\lambda_1 + \Delta\lambda + \dot{\lambda})\bar{\mathbf{f}}\right)\,, \tag{12}$$

and, then, by using Eq. (11), $\dot{\lambda}$

$$\dot{\lambda} = \frac{\Delta\mathbf{u}^T\mathbf{C}\mathbf{K}^{-1}_{\mathbf{u}_1+\Delta\mathbf{u}}(\mathbf{s}_{\mathbf{u}_1+\Delta\mathbf{u}} + (\lambda_1 + \Delta\lambda)\bar{\mathbf{f}})}{\gamma\Delta\lambda - \Delta\mathbf{u}^T\mathbf{C}\mathbf{K}^{-1}_{\mathbf{u}_1+\Delta\mathbf{u}}\mathbf{s}_{\mathbf{u}_1+\Delta\mathbf{u}}}\,. \tag{13}$$

At this point, we can specify $(\gamma, \mathbf{C})$ assuming the pair $(0, \mathbf{K})$ and, as a consequence, obtaining a very simple correction formula for $\Delta\lambda$:

$$\dot{\lambda} = -\frac{\Delta\mathbf{u}^T(\mathbf{s}_{\mathbf{u}_1+\Delta\mathbf{u}} + (\lambda_1 + \Delta\lambda)\bar{\mathbf{f}})}{\Delta\mathbf{u}^T\mathbf{s}_{\mathbf{u}_1+\Delta\mathbf{u}}}\,, \tag{14}$$

whereas the correction displacement vector $\dot{\mathbf{u}}$ for the extrapolation $\Delta\mathbf{u}$ can be computed by using Eq. (12).

The algorithm sketched in the immediate foregoing requires to define the first extrapolation in each step. The simplest way is to define it on the basis of the previous steps results. Using the already introduced symbols:

$$\begin{aligned}\Delta\lambda &= m(\lambda_1 - \lambda_0)\,,\\ \Delta\mathbf{u} &= m(\mathbf{u}_1 - \mathbf{u}_0)\,,\end{aligned} \tag{15}$$

where the coefficient m modifies, in an adaptive way, the arc-length when the step-by-step procedure goes ahead. More precisely, m increases the step-length in the parts of the equilibrium path rather linear and decreases the step-length in the parts of the equilibrium path which contain, e.g., limit point and hence require much more care. Following [54], the adaptive coefficient m can be computed as

$$m = 1 - \frac{r_l - n_l}{r_l + n_l}\,, \tag{16}$$

on the basis of r_l, required, and n_l, needed, number of loops to achieve the convergence. At the first step, we can set $m = 1$ and fix in advance the value of $\Delta\lambda$, defining the arc-length in an implicit way, from which the corresponding value of $\Delta\mathbf{u}$ can be computed.

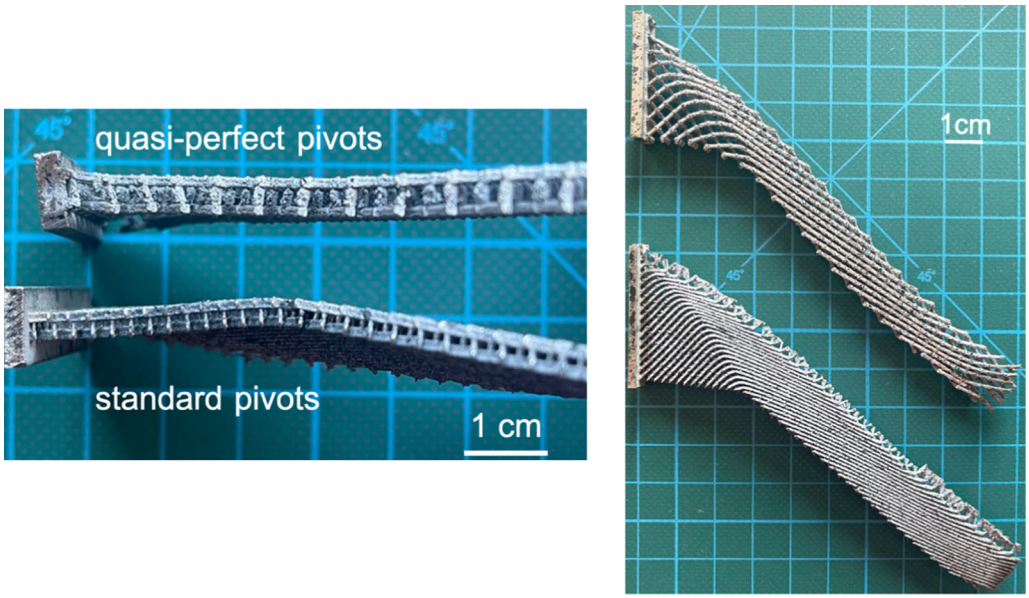

Fig. 4 Standard versus quasi-perfect pivots: comparison of deformed specimens in shear test [55]

4 Modeling of damage behavior via hemivariational formulation

In shear tests of pantographic layers, out-of-plane deformations may be significant affecting the overall mechanical behavior. As explained by Spagnuolo et al. [55] in detail, stiffnesses associated with each energy term play a crucial role, and indeed, depending on the considered set of stiffnesses, one deformation mechanism which results in an energy minimum is favored over another, for the same prescribed displacement. In shear tests of standard pantographic layers, it is generally observed that out-of-plane deformations occur due to high torsional stiffness of pivots, and to alleviate out-of-plane deformations, “quasi-perfect" pivots may be preferred. Experimental studies (see Fig. 4) show that, quasi-perfect pivots may modify significantly the overall behavior in terms of out-of-plane deformations. As can be clearly seen from Fig. 4, the pantographic layer with quasi-perfect pivots does not have any significant out-of-plane deformation compared to the one with standard pivots (please, see Spagnuolo et al. [55] for further discussion on the quasi-perfect pivots and their usage).

Besides, in the comparison of force–displacement plots (see Fig. 5), differences are observed due to the presence of quasi-perfect pivots. Importantly, from a qualitative point of view, similar trends are observed in both cases. The curve starts with a certain slope. Then, for a certain displacement step, the slope decreases considerably. At the end, the slope increases again, this time almost asymptotically, just before the first observed break. Here, it must be remarked that the effect of quasi-perfect pivots is ensured by reducing the torsional stiffness in the simulations [55].

In shear test, the first part of the deformation process of the pantographic structures is characterized by torsional deformation of the pivots from an energetic point of view, so the initial slope is strongly related to the torsional stiffness of the pantographic layer. In the second part, the angle between the fibers of the two families approaches zero with high displacements, i.e., fibers become parallel, and then the prevalent deformation mechanism becomes the elongation of the fibers. The activation of the deformation mechanism by fiber extension corresponds to the second change in slope observed in Fig. 5.

In this study, the existing 2D discrete model is improved including damage for each considered mechanism in the model (torsion of pivots, bending and elongation of fibers). In order to verify and validate the damage behavior, experimental measurements in the shear test of metallic pantographic layer made of quasi-perfect pivots are used as reference (see Fig. 5). As the current algorithm is two-dimensional, the pantographic layer made of standard pivots is not considered in this study due to excessive out-of-plane deformation.

In order to model damage behavior in the 2D discrete model, the approach presented in Sessa et al. [56] for linear springs is utilized and extended for also rotational springs. By following their study, for linear and

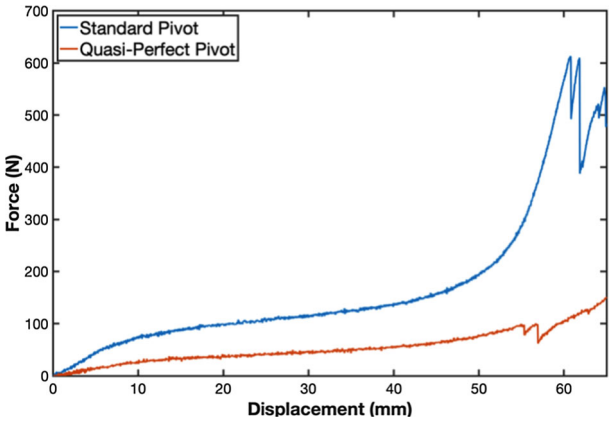

Fig. 5 Standard versus quasi-perfect pivots: comparison of experimentally measured force–displacement plots [55]

extensional springs, elastic energy is modified and a dissipation energy is introduced as follows:

$$w_{el}^{e} = \frac{1}{2}k_{el}^{e}(1-d_e)u^2, \qquad w_{diss}^{e} = \frac{1}{2}k_{d}^{e}\,d_e^2 + k_{t}^{e}d_e \tag{17}$$

where u is the deflection, $u = \left(\|p_j - p_i\| - \varepsilon\right)$, d_e is the damage term due to extension, where $d_e \in [0,1]$, and k_d^e and k_t^e are the damage parameters which control the evolution of the damage term d_e. The evolution of the extensional damage parameter can be obtained by the non-healing constraint on the damage and the so-called Karush–Kuhn–Tucker condition [56],

$$d_e(u) = \left(\frac{k_{el}^{e}u^2}{2k_{d}^{e}} - \frac{k_{t}^{e}}{k_{d}^{e}}\right) H\left(\frac{k_{el}^{e}u^2}{2k_{d}^{e}} - \frac{k_{t}^{e}}{k_{d}^{e}}\right) \tag{18}$$

where $H(x)$ is the Heaviside function.

Similarly, for rotational springs (for those used for bending and shear), we can follow the same idea and use the following elastic and dissipation energy terms:

$$w_{el}^{b} = k_{el}^{b}(1-d_b)\,(\cos\gamma_b + 1) \qquad w_{diss}^{b} = \frac{1}{2}k_{d}^{b}\,d_b^2 + k_{t}^{b}d_b, \tag{19}$$

$$w_{el}^{s} = \frac{1}{2}k_{el}^{s}(1-d_s)\left(\gamma_s - \frac{\pi}{2}\right)^2 \qquad w_{diss}^{s} = \frac{1}{2}k_{d}^{s}\,d_s^2 + k_{t}^{s}d_s. \tag{20}$$

Then, the hemivariational approach is utilized to obtain the evolution functions of the damage terms d_b and d_s as follows:

$$d_b(\gamma_b) = \left(\frac{k_{el}^{e}\,(\cos\gamma_b + 1)}{k_{d}^{e}} - \frac{k_{t}^{e}}{k_{d}^{e}}\right) H\left(\frac{k_{el}^{e}\,(\cos\gamma_b + 1)}{k_{d}^{e}} - \frac{k_{t}^{e}}{k_{d}^{e}}\right), \tag{21}$$

$$d_s(\gamma_s) = \left(\frac{k_{el}^{s}{\gamma_s}^2}{2k_{d}^{s}} - \frac{k_{t}^{s}}{k_{d}^{s}}\right) H\left(\frac{k_{el}^{s}{\gamma_s}^2}{2k_{d}^{s}} - \frac{k_{t}^{s}}{k_{d}^{s}}\right). \tag{22}$$

Finally, with this modification, the solution procedure explained in previous section is utilized by including elastic and dissipation energy terms inside Eq. 5 to investigate damage behavior in pantographic layers. Each damage term (d_e, d_b, or d_s) is evaluated and updated according to corresponding Karush–Kuhn–Tucker condition in each load step, identifying degradation for each type of spring used in the discrete system (Eqs. 18, 21 and 22). Importantly, the k_t terms identify the threshold energy value to activate damage, while k_d terms characterize how fast the activated damage propagates in the simulation.

Table 1 Stiffness and damage parameters used in numerical simulations

Parameter	Value	Parameter	Value	Parameter	Value
k^e_{el}	8×10^5 N/m	k^b_{el}	0.46 Nm	k^s_{el}	0.035 Nm
k^e_t	4.65	k^b_t	1E-5	k^s_t	2.1E-5
k^e_d	1.8	k^b_d	0.55	k^b_d	7.5E-4

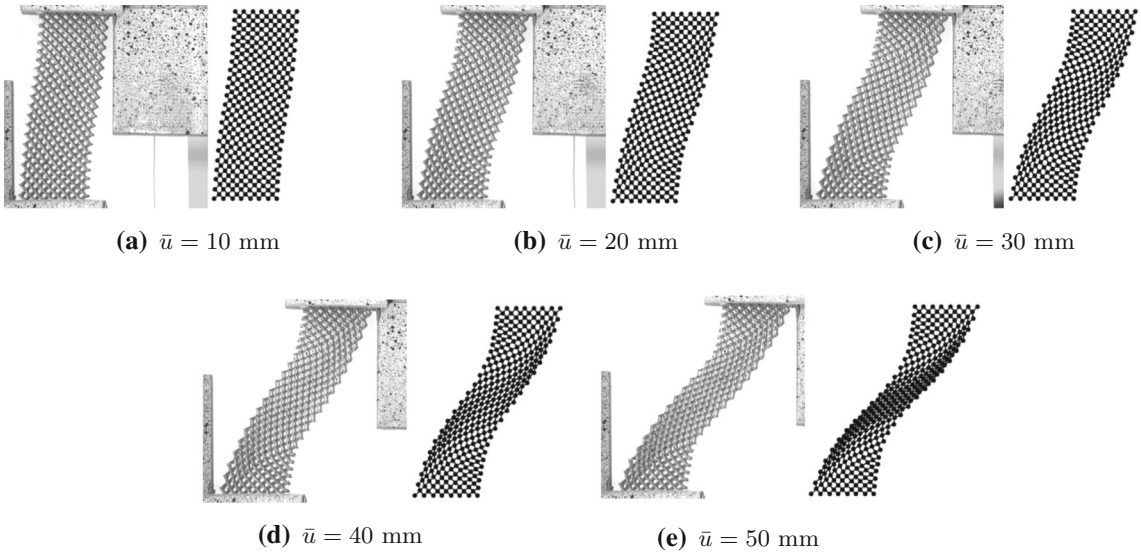

(a) $\bar{u} = 10$ mm **(b)** $\bar{u} = 20$ mm **(c)** $\bar{u} = 30$ mm

(d) $\bar{u} = 40$ mm **(e)** $\bar{u} = 50$ mm

Fig. 6 Comparison of deformed configurations: experiment versus simulation

5 Numerical results and comparisons

In this section, the presented mathematical framework is examined with a metallic pantographic layer under shear test. The pantographic layer has fibers of width $a = 1$ mm and depth $b = 1$ mm, and quasi-perfect pivots of radius $r = 0.4$ mm and height $h = 1.5$ mm. The number of fibers along its width (ℓ) is $N_f = 7$. The structure has been investigated by Spagnuolo et al. [55] using a 2D second-gradient model accounting out-of-plane deformations with a simplified damage approach. In Spagnuolo et al. [55], damage was only taken into account for quasi-perfect pivots, and it was assumed that a significant degradation occurs if the rotation threshold is exceeded. In this study, we investigate the same behavior using a discrete model and including damage not only for torsion of pivots but also for bending and extension of fibers. In numerical simulations, to include damage behavior of the specimen during shear test, the parameters listed in Table 1 were adopted, and a 75-mm prescribed displacement ($\bar{u}$) was applied in 300 steps to the top side of the specimen.

In Fig. 6, the obtained deformed configurations are compared to those observed in the experiment for prescribed displacements, $\bar{u} = 10, 20, 30, 40$ and 50 mm. As can be seen from the comparison, the experimental and numerical deformed shapes compare each other very well. As discussed in previous section, according to experimental measurements, we expect that the first part of the deformation is characterized by the torsional behavior of quasi-perfect pivots, i.e., damage in shear springs. Here, it must be remarked that although it is possible to design perfect pivot in a CAD software (pivot with zero torsional resistance), it is still a challenging fabrication process due to many possible 3D printing issues that may occur. Therefore, the printed pivots are referred to as “quasi-perfect" which indicates low torsional stiffness, and this stiffness is significant early in the deformation process.

In Fig. 7, experimental and numerical reaction force–displacement plots are compared. The comparison shows that the adopted damage parameters ($k^e_t, k^e_d, k^b_t, k^b_d, k^s_t, k^s_d$) provide the expected behavior in the numerical simulation, and the two plots show a close match. Here, in order to get more insight, it is crucial to understand how damage evolves in both pivots and fibers (torsion of pivots, bending and extension of fibers) as the occurring damage highly affects the overall behavior of the pantographic structure.

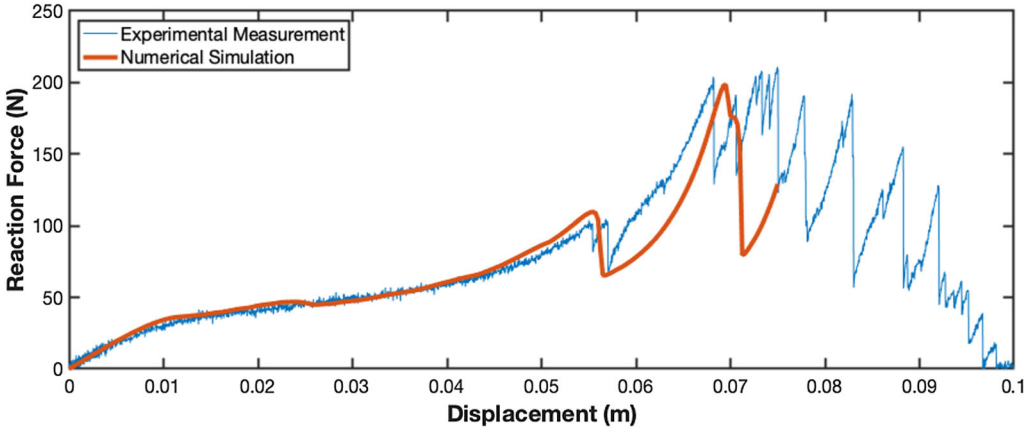

Fig. 7 Comparison of reaction force at the fixed side: experiment versus simulation

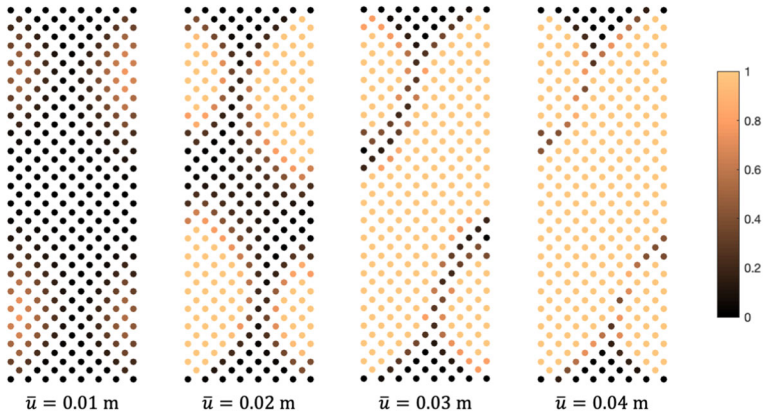

Fig. 8 Damage evolution due to torsion of pivots

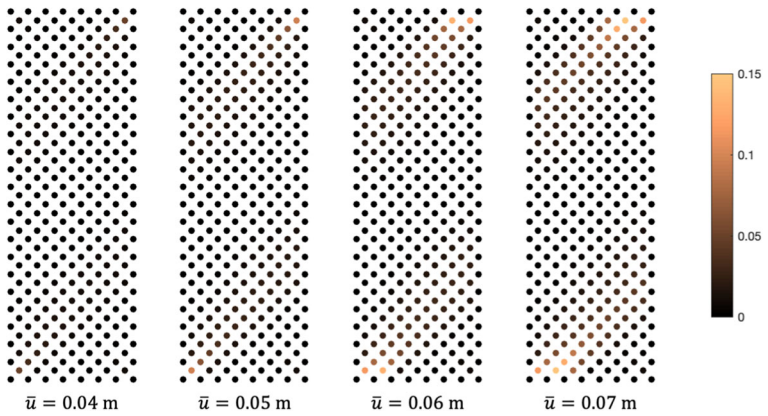

Fig. 9 Damage evolution due to bending of fibers

In order to comprehend the first part of the reaction force–displacement graph, damage evolution due to torsional behavior of pivots are presented in Fig. 8. Here, the contour plot is given for the damage parameter d_s ($d_s = 0$ no damage, $d_s = 1$ fully damaged), for prescribed displacements $\bar{u} = 10$, 20, 30 and 40 mm. As can be clearly seen from Fig. 8, damage parameters of most pivots (d_s) reach to 1 in the beginning of simulation, and this clearly explains how the first slope change in reaction force–displacement plot is obtained.

Next, to elucidate the second part of the reaction force–displacement graph, damage evolutions due to bending and extension of fibers are, respectively, presented in Fig. 9 and 10. In both figures, results are

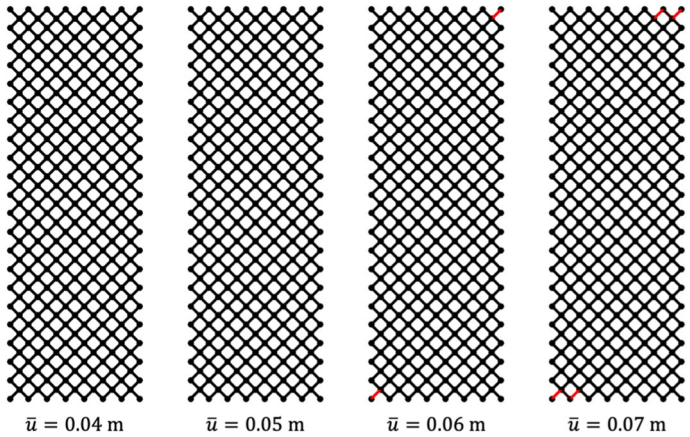

Fig. 10 Damage evolution due to extension of fibers (red fibers are the ones fully damaged)

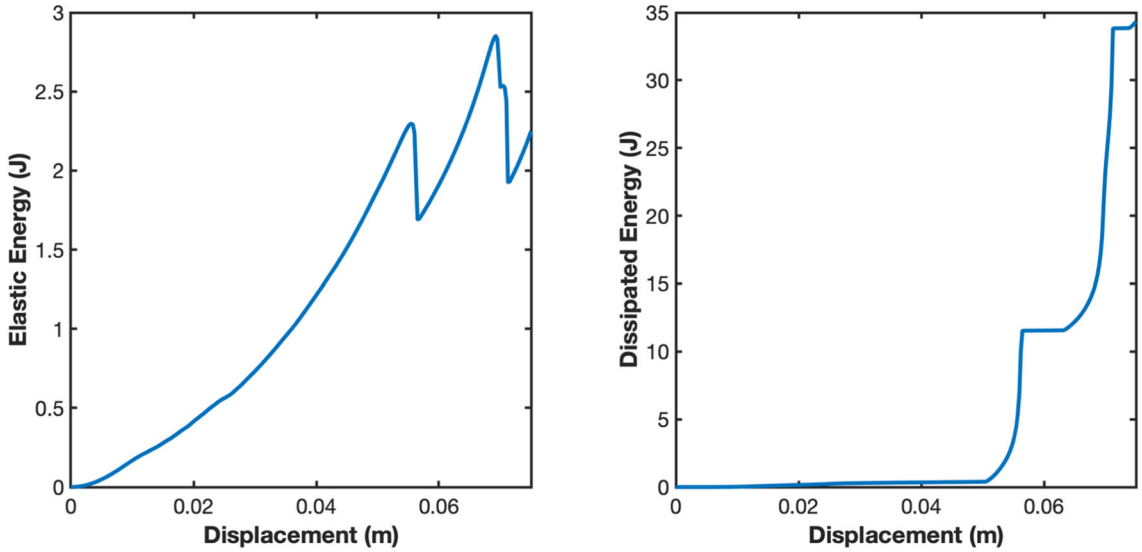

Fig. 11 Elastic energy versus dissipated energy during simulation

provided for prescribed displacements, $\bar{u} = 40, 50, 60,$ and 70 mm. During the numerical simulation, Fig. 9 shows that damage due bending of fibers does not reach to 1 (fully damaged). Indeed, this investigation can be supported by the damaged specimen at the end of experiment given in Fig. 4 as there is no fully damaged fiber due to bending. On the other hand, the sudden jumps start to occur significantly after 60 mm, due to damage in the extension of fibers. According to the numerical simulation, the fibers on the short sides first get fully damaged. This again can be explained by using the experimental observation: in the experiment fibers on the top side get fully damage as can be seen in Fig. 4. Here, it must be noted that in the study presented by Spagnuolo et al. [55] the second part of the force–displacement plot cannot be captured as the study only focuses on damage in quasi-perfect pivots.

Moreover, the computed total elastic ($w^e_{el} + w^b_{el} + w^s_{el}$) and dissipation ($w^e_{diss} + w^b_{diss} + w^s_{diss}$) energies are given as functions of prescribed displacement in Fig. 11. Here, as it is expected, the dissipation energy is always increasing due to irreversibility of damage terms. Also, it is observed that there is no significant dissipation energy increase in the beginning of simulation. However, around 0.05 m, dissipation energy starts to increase considerably, due to the observed failure in extensional springs (see Fig. 10). On the other hand, jumps in elastic energy shows that failure of extensional springs in the specimen activates other springs and elastic energy increases again after a certain drop.

6 Conclusions

In summary, we have provided an hemivariational formulation for those discrete elements that are included in an Hencky-type discrete model that was conceived for pantographic layers. In order to model damage and fracture behavior of such pantographic layer, three damage kinematic descriptors have been added for those three kinds of springs included in the elastic model. Euler-Lagrange equations aimed to the evolution of the displacements of the internal pivots and Karush–Khun–Tucker conditions aimed to govern the evolution of damage descriptors have been derived from an hemivariational principle and numerically investigated with an efficient and smart strategy able to solve the nonlinear equilibrium equations coupled with the evolution of damage variables. The 6 constitutive parameters of the 3 kinds of springs (2 per each kind of spring, the first corresponding to the activation of damage and the second prescribing the velocity of damage evolution until fracture) have been identified with a comparison with an experimental data available in the literature.

Funding No funding was received for conducting this study.

Declarations

Competing interest The authors have no competing interests to declare that are relevant to the content of this article.

References

1. Yildizdag, M.E., Tran, C.A., Barchiesi, E., Spagnuolo, M., dell'Isola, F., Hild, F.: A multi-disciplinary approach for mechanical metamaterial synthesis: a hierarchical modular multiscale cellular structure paradigm. In: State of the Art and Future Trends in Material Modeling, pp. 485–505. Springer (2019)
2. Vangelatos, Z., Komvopoulos, K., Grigoropoulos, C.: Vacancies for controlling the behavior of microstructured three-dimensional mechanical metamaterials. Math. Mech. Solids **24**(2), 511–524 (2019)
3. Berezovski, A., Yildizdag, M.E., Scerrato, D.: On the wave dispersion in microstructured solids. Continuum Mech. Thermodyn. **32**(3), 569–588 (2020)
4. Kwon, J., Evans, K., Ma, L., Arnold, D., Yildizdag, M.E., Zohdi, T., Ritchie, R.O., Xu, T.: Scalable electrically conductive spray coating based on block copolymer nanocomposites. ACS Appl. Mater. Interfaces **12**(7), 8687–8694 (2020)
5. Spagnuolo, M., Cazzani, A.M.: Contact interactions in complex fibrous metamaterials. Contin. Mech. Thermodyn. 1–17 (2021)
6. Vangelatos, Z., Yildizdag, M.E., Giorgio, I., dell'Isola, F., Grigoropoulos, C.: Investigating the mechanical response of microscale pantographic structures fabricated by multiphoton lithography. Extr. Mech. Lett. **43**, 101202 (2021)
7. Barchiesi, E., Spagnuolo, M., Placidi, L.: Mechanical metamaterials: a state of the art. Math. Mech. Solids **24**(1), 212–234 (2019)
8. Eremeyev, V.A., Boutin, C., Steigmann, D., et al.: Linear pantographic sheets: existence and uniqueness of weak solutions. J. Elast. **132**(2), 175–196 (2018)
9. dell'Isola, F., Turco, E., Misra, A., Vangelatos, Z., Grigoropoulos, C., Melissinaki, V., Farsari, M.: Force-displacement relationship in micro-metric pantographs: experiments and numerical simulations. Comptes Rendus Mécanique **347**(5), 397–405 (2019)
10. Desmorat, B., Spagnuolo, M., Turco, E.: Stiffness optimization in nonlinear pantographic structures. Math. Mech. Solids **25**(12), 2252–2262 (2020)
11. Yildizdag, M.E., Barchiesi, E., dell'Isola, F.: Three-point bending test of pantographic blocks: numerical and experimental investigation. Math. Mech. Solids **25**(10), 1965–1978 (2020)
12. Auger, P., Lavigne, T., Smaniotto, B., Spagnuolo, M., dell'Isol F., Hild, F.: Poynting effects in pantographic metamaterial captured via multiscale DVC. The J. Strain Anal. Eng. Des. **56**(7), 462–477 (2021)
13. Eremeyev, V.A., Ganghoffer, J.-F., Konopińska-Zmysłowska, V., Uglov, N.S.: Flexoelectricity and apparent piezoelectricity of a pantographic micro-bar. Int. J. Eng. Sci. **149**, 103213 (2020)
14. Spagnuolo, M., Andreaus, U., Misra, A., Giorgio, I., Hild, F.: Mesoscale modeling and experimental analyses for pantographic cells: effect of hinge deformation. Mech. Mater. **160**, 103924 (2021)
15. dell'Isola, F., Seppecher, P., Alibert, J.-J., Lekszycki, T., Grygoruk, R., Pawlikowski, M., Steigmann, D., Giorgio, I., Andreaus, U., Turco, E., et al.: Pantographic metamaterials: an example of mathematically-driven design and of its technological challenges. Continuum Mech. Thermodyn. **31**(4), 851–884 (2019)
16. dell'Isola, F., Seppecher, P., Spagnuolo, M., Barchiesi, E., Hild, F., Lekszycki, T., Giorgio, I., Placidi, L., Andreaus, U., Cuomo, M., Eugster, S.R., et al.: Advances in pantographic structures: design, manufacturing, models, experiments and image analyses. Contin. Mech. Thermodyn. **31**(4), 1231–1282 (2019)
17. dell'Isola, F., Andreaus, U., Placidi, L.: At the origins and in the vanguard of peridynamics, non-local and higher-gradient continuum mechanics: an underestimated and still topical contribution of gabrio piola. Math. Mech. Solids **20**(8), 887–928 (2015)

18. dell'Isola, F., Corte, A.D., Giorgio, I.: Higher-gradient continua: the legacy of piola, mindlin, sedov and toupin and some future research perspectives. Math. Mech. Solids **22**(4), 852–872 (2017)
19. Giorgio, I., Della Corte, A., dell'Isola, F., Steigmann, D.J.: Buckling modes in pantographic lattices. C. R. Mec. **344**(7), 487–501 (2016)
20. Giorgio, I., Varano, V., dell'Isola, F., Rizzi, N.L.: Two layers pantographs: a 2d continuum model accounting for the beams? Offset and relative rotations as averages in so (3) lie groups. Int. J. Solids Struct. **216**, 43–58 (2021)
21. Giorgio, I.: Lattice shells composed of two families of curved kirchhoff rods: an archetypal example, topology optimization of a cycloidal metamaterial. Contin. Mech. Thermodyn. **33**(4), 1063–1082 (2021)
22. Placidi, L.: A variational approach for a nonlinear 1-dimensional second gradient continuum damage model. Contin. Mech. Thermodyn. **27**(4), 623–638 (2015)
23. Placidi, L., Misra, A., Barchiesi, E.: Two-dimensional strain gradient damage modeling: a variational approach. Zeitschrift für angewandte Math. und Phys. **69**(3), 1–19, (2018)
24. Placidi, L., Barchiesi, E., Misra, A.: A strain gradient variational approach to damage: a comparison with damage gradient models and numerical results. Math. Mech. Compl. Syst. **6**(2), 77–100 (2018)
25. Abali, B.E., Klunker, A., Barchiesi, E., Placidi, L.: A novel phase-field approach to brittle damage mechanics of gradient metamaterials combining action formalism and history variable. ZAMM-J. Appl. Math Mech./Zeitschrift für Angewandte Math. Mech. **101**(9), e202000289.
26. Barchiesi, E., Yang, H., Tran, C., Placidi, L., Müller, W.H.: Computation of brittle fracture propagation in strain gradient materials by the fenics library. Math. Mech. Solids **26**(3), 325–340 (2021)
27. Timofeev, D., Barchiesi, E., Misra, A., Placidi, L.: Hemivariational continuum approach for granular solids with damage-induced anisotropy evolution. Math. Mech. Solids **26**(5), 738–770 (2021)
28. Placidi, L.: A variational approach for a nonlinear one-dimensional damage-elasto-plastic second-gradient continuum model. Contin. Mech. Thermodyn. **28**(1–2), 119–137 (2016)
29. Placidi, L., Barchiesi, E., Misra, A., Timofeev, D.: Micromechanics-based elasto-plastic-damage energy formulation for strain gradient solids with granular microstructure. Contin. Mech. Thermodyn. **33**(5), 2213–2241 (2021)
30. Steigmann, D.: Gradient plasticity in isotropic solids. Math. Mech. Solids. **27**(10), 1896–1912 (2021)
31. Abali, B.E., Barchiesi, E.: Additive manufacturing introduced substructure and computational determination of metamaterials parameters by means of the asymptotic homogenization. Contin. Mech. Thermodyn. **33**(4), 993–1009 (2021)
32. Barchiesi, E., Misra, A., Placidi, L., Turco, E.: Granular micromechanics-based identification of isotropic strain gradient parameters for elastic geometrically nonlinear deformations. ZAMM-J. Appl. Math. Mech./Zeitschrift für Angewandte Math. Mech. **101**(11), e202100059. (2021)
33. Spagnuolo, M., Yildizdag, M.E., Andreaus, U., Cazzani, A.M.: Are higher-gradient models also capable of predicting mechanical behavior in the case of wide-knit pantographic structures? Math. Mech. Solids **26**(1), 18–29 (2021)
34. Yang, H., Timofeev, D., Abali, B.E., Li, B., Müller, W.H.: Verification of strain gradient elasticity computation by analytical solutions. ZAMM-J. Appl. Math. Mech./Zeitschrift für Angewandte Math. Mech. **101**(12), e202100023 (2021)
35. Andreaus, U., Spagnuolo, M., Lekszycki, T., Eugster, S.R.: A ritz approach for the static analysis of planar pantographic structures modeled with nonlinear euler-bernoulli beams. Contin. Mech. Thermodyn. **30**(5), 1103–1123 (2018)
36. Spagnuolo, M., Barcz, K., Pfaff, A., dell'Isola, F., Franciosi, P.: Qualitative pivot damage analysis in aluminum printed pantographic sheets: numerics and experiments. Mech. Res. Commun. **83**, 47–52 (2017)
37. Spagnuolo, M., Peyre, P., Dupuy, C.: Phenomenological aspects of quasi-perfect pivots in metallic pantographic structures. Mech. Res. Commun. **101**, 103415 (2019)
38. dell'Isola, F., Giorgio, I., Pawlikowski, M., Rizzi, N.L.: Large deformations of planar extensible beams and pantographic lattices: heuristic homogenization, experimental and numerical examples of equilibrium. Proc. Royal Soc. A: Math. Phys. Eng. Sci. **472**(2185), 20150790 (2016)
39. Boutin, C., Giorgio, I., Placidi, L., et al.: Linear pantographic sheets: asymptotic micro-macro models identification. Math. Mech. Compl. Syst. **5**(2), 127–162 (2017)
40. Giorgio, I., Rizzi, N., Turco, E.: Continuum modelling of pantographic sheets for out-of-plane bifurcation and vibrational analysis. Proc. R. Soc. A: Math. Phys. Eng. Sci. **473**(2207), 20170636 (2017)
41. Giorgio, I.: Numerical identification procedure between a micro-cauchy model and a macro-second gradient model for planar pantographic structures. Z. Angew. Math. Phys. **67**(4), 1–17 (2016)
42. Turco, E., dell'Isola, F., Cazzani, A., Rizzi, N.L.: Hencky-type discrete model for pantographic structures: numerical comparison with second gradient continuum models. Z. Angew. Math. Phys. **67**(4), 1–28 (2016)
43. Turco, E.: Discrete is it enough? the revival of Piola-Hencky keynotes to analyze three-dimensional Elastica. Contin. Mech. Thermodyn. **30**(5), 1039–1057 (2018)
44. Turco, E., Misra, A., Pawlikowski, M., dell'Isola, F., Hild, F.: Enhanced Piola-Hencky discrete models for pantographic sheets with pivots without deformation energy: numerics and experiments. Int. J. Solids Struct. **147**, 94–109 (2018)
45. Turco, E., Barchiesi, E., Giorgio, I., dell'Isola, F.: A lagrangian Hencky-type non-linear model suitable for metamaterials design of shearable and extensible slender deformable bodies alternative to Timoshenko theory. Int. J. Non-Linear Mech. **123**, 103481 (2020)
46. Turco, E.: A numerical survey of nonlinear dynamical responses of discrete pantographic beams. Contin. Mech. Thermodyn. **33**(4), 1465–1485 (2021)
47. Turco, E., Golaszewski, M., Giorgio, I., D'Annibale, F.: Pantographic lattices with non-orthogonal fibres: experiments and their numerical simulations. Compos. B Eng. **118**, 1–14 (2017)
48. Hencky, H.: Über die angenäherte lösung von stabilitätsproblemen im raum mittels der elastischen gelenkkette. PhD thesis, Verlag nicht ermittelbar (1921)
49. Challamel, N., Kocsis, A., Wang, C.: Discrete and non-local elastica. Int. J. Non-Linear Mech. **77**, 128–140 (2015)
50. Wang, C.M., Zhang, H., Gao, R., Duan, W., Challamel, N.: Hencky bar-chain model for buckling and vibration of beams with elastic end restraints. Int. J. Struct. Stab. Dyn. **15**(07), 1540007 (2015)

51. Riks, E.: An incremental approach to the solution of snapping and buckling problems. Int. J. Solids Struct. **15**(7), 529–551 (1979)
52. Turco, E., Caracciolo, P.: Elasto-plastic analysis of Kirchhoff plates by high simplicity finite elements. Comput. Methods Appl. Mech. Eng. **190**(5–7), 691–706 (2000)
53. Barchiesi, E., dell'Isola, F., Bersani, A.M., Turco, E.: Equilibria determination of elastic articulated duoskelion beams in 2D via a Riks-type algorithm. Int. J. Non-Linear Mech. **128**, 103628 (2021)
54. Clarke, M.J., Hancock, G.J.: A study of incremental-iterative strategies for non-linear analyses. Int. J. Numer. Meth. Eng. **29**(7), 1365–1391 (1990)
55. Spagnuolo, M., Yildizdag, M.E., Pinelli, X., Cazzani, A., Hild, F.: Out-of-plane deformation reduction via inelastic hinges in fibrous metamaterials and simplified damage approach. Math. Mech. Solids. **27**(6), 1011–1031 (2022)
56. Sessa, S., Barchiesi, E., Placidi, L., Paradiso, M., Turco, E., Hamila, N.: An insight into computational challenges in damage mechanics: analysis of a softening Hooke's spring. In: Giorgio, I., Placidi, L., Barchiesi, E., Abali, B.E., Altenbach, H. (eds.) Theoretical Analyses, Computations, and Experiments of Multiscale Materials: A Tribute to Francesco dell'Isola, pp. 537–564, Springer (2022)